(23) Termonia, Y.; Smith, P. In *High Modulus Polymers*; Zachariades, A. E.; Porter, R. S., Eds.; Marcel Dekker Inc.: New York, 1988, Chapter 11.
(24) Halpin, J. C.; Kardos, J. L. *Polym. Eng. Sci.* **1976**, *16*, 344.
(25) He, T. *Polymer* **1986**, *27*, 253.
(26) Aharoni, S. M. *Macromolecules* **1981**, *14*, 222.
(27) Tashiro, K.; Tadakoro, H. *Macromolecules* **1978**, *11*, 914.
(28) Postema, A. R.; Smith, P. *Macromolecules*, in press.

Registry No. PHIC (homopolymer), 26746-07-6; PHIC (SRU), 37727-37-0.

On the Relation between Structure and Dynamics of Star Polymers in Dilute Solution

D. Richter* and B. Farago

Institut Laue Langevin, 38000 Grenoble, France

L. J. Fetters and J. S. Huang

Exxon Research & Engineering Co., Annandale, New Jersey 08801

B. Ewen

Max Planck Institut für Polymerforschung, 6500 Mainz, FRG. *Received July 14, 1989; Revised Manuscript Received October 4, 1989*

ABSTRACT: Studying star polymers in solution, where the inner core, the outer shell, or the full star was labeled, we investigated in detail the relation between the architecture of a star polymer and its initial dynamic response. In the framework of the RPA approach we evaluate the initial relaxation rates for the inner and outer part of a Gaussian star including the hydrodynamic interaction. Furthermore, we point out a general relation between the structure of stars with arbitrary arm statistics and their dynamic response. We present small-angle neutron scattering data on 12-arm partially and fully labeled polyisoprene stars and evaluate the corresponding partial structure factors. The best description of these data is given by the recent molecular dynamics simulations. The star dynamics were investigated by neutron spin–echo spectroscopy. The relaxation behavior of the star core and shell were found to differ qualitatively. While the reduced relaxation rates of the star core as well as of a fully labeled star undergo a pronounced minimum at intermediate Q values, the respective shell relaxation rates undergo a maximum in the same Q range. On the basis of the measured partial and full static structure factors within the random-phase approximation (RPA) approach, the Q dependence of the initial star relaxation rates under all contrast conditions can be quantitatively accounted for. On the other hand, the time scales of the relaxation process reflect also dynamic features such as hydrodynamic screening. At longer times further dynamic processes like the disentangling of interarm entanglements appear to come into play.

I. Introduction

Long flexible polymers in dilute solutions have been a subject of long-standing interest from both an experimental and a theoretical point of view.[1,2] While the static and dynamic properties of linear chains have been widely investigated and appear to be well understood, much less is known on branched polymers. Star polymers, where several linear chain molecules of nearly identical molecular weight are attached at one end to a center molecule, may be considered as prototype materials for branched systems. The star structure implies a very inhomogeneous polymer density profile: starting from the crowded star center, where we have to consider strongly stretched chains, the density profile decreases to the outer regions of the star. If scaling ideas are introduced, according to Daoud and Cotton[3] and Birshtein et al. this may be pictured in terms of the concept of semidilute solutions with a blob size decreasing from the rim to the center. Explicit calculations on the star structure are available for Gaussian stars,[6] while molecular dynamics calculations yielded results for real systems.[7] The internal star dynamics have been treated on the level of initial slope calculations on the basis of Kirkwood's diffusion equation, which takes into account the hydrodynamic interaction between chain segments.[6] These calculations are also available for partially labeled systems like stars built from diblock copolymers of different scattering contrast.[8] Lately, considerations on the structure and dynamics of diblock copolymers of arbitrary architecture put these calculations into a general context.[8–11]

On the other hand, progress in anionic polymerization made it possible to synthesize star polymers with a narrow distribution of molecular weight and functionality.[12] These achievements triggered intense experimental efforts to investigate these well-characterized, monodisperse, branched polymers. Elastic light scattering,[13] small-angle neutron (SANS),[14] and X-ray scattering[15] addressed structural aspects, while quasielastic light scattering[13] and NMR[16] dealt with diffusional prop-

* Address correspondence to this author at Inst. für Festkörperforschung, Kernforschungsanlage Jülich, 5170 Jülich, FRG.

0024-9297/90/2223-1845$02.50/0

erties. Quasielastic neutron scattering (QNS)[14,17] allowed access to the internal chain dynamics. Concerning the evaluation of structural details as well as the study of the internal star dynamics, neutron scattering is practically a unique probe. This is partly due to the fact that by hydrogen–deuterium isotope exchange the scattering contrast can be changed at will, allowing one to observe structural and dynamical properties of selected parts of the star. Second, since with cold neutrons the accessible momentum and energy transfers correspond to intramolecular distances *and* relaxation times, QNS accesses simultaneously the space *and* time evolution of the intramolecular motion.

Recently, Richter et al.[14] reported SANS and neutron spin–echo experiments on the structure and dynamics of polyisoprene (PI) stars in dilute solution, which revealed a close relation between star architecture and star dynamics. For a given functionality f the small-angle scattering data were found to scale with $Q\tilde{R}_g$, where $\tilde{R}_g$ is the radius of gyration of one arm and Q the momentum transfer during scattering. While in a Kratky representation ($I(Q)Q^{1/\nu}$ versus Q; ν, Flory exponent) the scattering intensity $I(Q)$ from a linear polymer increases smoothly from zero at $Q = 0$ to a high-Q plateau, in the case of star molecules a pronounced maximum around $Q\tilde{R}_g \simeq 1.2$ was observed, the height of which increases with increasing functionality. Its occurrence is related to an enhancement of the radial segment distribution function of a star compared to a linear chain. This effect is most pronounced at distances $r \sim \tilde{R}_g$.

The internal star dynamics are most conveniently discussed in terms of reduced relaxation rates $\Omega(Q)/Q^3$, thus taking out the ordinary Zimm relaxation ($\Omega \sim Q^3$). As for the static data it was found that the reduced rates for different high-functionality stars scale with $Q\tilde{R}_g$. Thereby, at high $Q\tilde{R}_g$ the results from all stars coincide with reduced rates found for a linear chain in the Zimm regime. This relaxation rate depends only on the friction term T/η_0, where T is the temperature and η_0 the solvent viscosity. At low Q the internal dynamics become invisible and only diffusive modes contribute to the relaxation behavior. Here again Ω/Q^3 was found to scale with $Q\tilde{R}_g$, exhibiting a weak dependence on functionality. Finally in the crossover regime from Zimm relaxation to translational diffusion behavior, where the reduced relaxation rate of a linear chain changes smoothly from Ω/Q^3 = constant to $\Omega/Q^3 \sim Q^{-1}$, the reduced rates of high-functionality stars traverse a deep minimum. This anomalous slowing down is observed in the neighbourhood of the maximum in the Kratky plot of the scaled elastic intensity. In analogy to the "de Gennes" narrowing[18] found in liquids, the observed retardation of the relaxation rate was interpreted as a collective phenomenon originating from the pairwise interaction of the different arms in the star structure. We emphasize that other than in the dynamics of liquids where the de Gennes narrowing results from the effect of interparticle correlations on the collective relaxation rate, the observed minimum in Ω/Q^3 is not related to interstar interactions but originates from the interactions of different parts in the same molecule. The collective nature of the minimum in the relaxation rate was proved in a further experiment on a star with a single labeled arm.[17] There, the minimum in the reduced rate is not found but a smooth and gradual crossover from the asymptotic Zimm dynamics to the low-Q diffusive behavior was observed.

So far we have developed a qualitative picture of the relation between star architecture and dynamics. It was the aim of the work reported here to investigate quantitatively how far the star structure predicts its dynamic response. We studied 12-arm PI stars made up of protonated/deuterated (H–D) diblock copolymers thus providing core–shell contrast. Experiments at three different contrasts lead to the determination of the partial static and dynamic structure factors. In addition we also studied a fully labeled star of the same size. The results are compared with different theoretical models based on the RPA approach brought forward by Benoit and others.[9–11] In the second section we define the partial structure factors, derive their equation of motion in random phase approximation, and give explicit solutions. Following the approach of Benoit and Hadziioannou,[9] we calculated the static structure factor for Gaussian and swollen (H–D) stars. Then, using a result of Kajiwara and Burchard[19] we present an expression for the mobility matrix containing a hydrodynamic interaction for a star of arbitrary conformation. The third section occupies itself with the sample preparation and characterization. Thereafter in the fourth section the SANS results are presented. From these data the partial static structure factors are derived. They are compared with the structure factors for Gaussian and swollen stars and with recent molecular dynamic simulations. In the fifth section we present our neutron spin–echo results. The experimentally observed relaxation behavior is related to the prediction of the RPA model for Gaussian stars and compared to RPA results for the dynamic response, which are obtained on the basis of the observed structure. Finally the relaxation dynamics of the inner star are set in relation to that of a fully labeled star of the same size as the diblock copolymer stars. The sixth section summarizes the obtained results and concludes this work.

II. Theoretical Considerations

II.1. Intermediate Scattering Cross Section. The double-differential coherent neutron cross section for an incompressible copolymer solution is given by

$$\frac{\partial^2\sigma}{\partial\theta\partial\omega} = \frac{\mathbf{k}_f}{\mathbf{k}_i} n \int \sum_{ij} a_i a_j \langle e^{i\mathbf{Q}\mathbf{r}_i(0)} e^{-i\mathbf{Q}\mathbf{r}_j(t)} \rangle e^{i\omega t}\, dt \qquad (1)$$

with

$$a_i = \left(\frac{b_p{}^i}{M_p{}^i}\rho_p - \frac{b_s}{M_s}\rho_s \right) \frac{M_p{}^i}{\rho_p}$$

Thereby $\mathbf{k}_i$ and $\mathbf{k}_f$ denote the momentum of the incoming and scattered neutron, respectively; θ is the solid angle in which the scattering takes place; ω is the energy transfer during scattering; n is the number of polymers; a_i is the scattering contrast between monomer "i" and the solvent, $b_p{}^i$ and b_s being the respective scattering lengths; $M_p{}^i$ and M_s are the atomic weights of the monomer "i" and the solvent molecule and $\rho_p{}^i$ and ρ_s their densities; and $\mathbf{Q} = \mathbf{k}_f - \mathbf{k}_i$ is the momentum transfer during scattering and $\mathbf{r}_j(t)$ the spatial coordinate of monomer "j" at time t. The sum has to be taken over all monomers i and j and the brackets denote the thermal average. For a diblock (A–B) copolymer we may define the partial intermediate dynamic structure factors

$$S_{\alpha\beta}(Q,t) = \sum_{ij} \langle e^{i\mathbf{Q}\mathbf{r}_{i\alpha}(0)} e^{-i\mathbf{Q}\mathbf{r}_{j\beta}(t)} \rangle \qquad (2)$$

where α and β denote the monomers of the blocks A and

B. With eq 2, eq 1 may be rewritten as

$$\frac{\partial^2\sigma}{\partial\theta\partial\omega} = \frac{\mathbf{k}_f}{\mathbf{k}_i} n \int \sum_{\alpha\beta} a_\alpha a_\beta S_{\alpha\beta}(Q,t) e^{i\omega t}\, dt \qquad (3)$$

In the framework of linear response theory the dynamic response functions $\chi_{\alpha\beta}(Q,t)$ are related to the intermediate scattering functions by[11]

$$k_B T \chi_{\alpha\beta}(Q,t) = -\frac{\partial}{\partial t} S_{\alpha\beta}(Q,t) \quad t \geq 0$$
$$= 0 \quad t < 0 \qquad (4)$$

where k_B is the Boltzmann constant and T the absolute temperature. If we neglect all memory effects in the calculation of the dynamic response, eq 4 facilitates the setup of simple equations of motion for the intermediate scattering function $S_{\alpha,\beta}(Q,t)$[20]

$$\frac{\partial}{\partial t} S_{\alpha\beta}(Q,t) + \sum_\gamma \Omega_{\alpha\gamma} S_{\gamma\beta}(Q,t) = 0 \qquad (5)$$

where Ω is the first cumulant matrix

$$\Omega = \lim_{t\to 0} \frac{\partial}{\partial t} \mathbf{S}(Q,t)\mathbf{S}^{-1}(Q) \qquad (6)$$

In terms of a generalized mobility matrix $\mathbf{M}(Q)$, which we will discuss later on in detail, Ω can also be written as[20]

$$\Omega = k_B T Q^2 \mathbf{M}(Q)\mathbf{S}^{-1}(Q) \qquad (7)$$

Equation 5 may be solved by the Laplace transformation

$$\mathbf{S}(Q,s) = [s\mathbf{E} + \Omega]^{-1}\mathbf{S}(Q,0) \qquad (8)$$

where $\mathbf{E}$ is the unity matrix.

The two eigenvalues describe the two different relaxation modes of the system

$$\Gamma_{1/2} = \Omega_{av} \mp (\Omega_{av}^2 - \Delta(\Omega))^{1/2} \qquad (9)$$

with

$$\Omega_{av} = {}^1/_2(\Omega_{11} + \Omega_{22})$$
$$\Delta\Omega = \Omega_{11}\Omega_{22} - \Omega_{12}\Omega_{21}$$

The eigenvectors determine the spectral weight of the relaxation modes in the scattering function. The final result for $S_{\alpha\beta}(Q,t)$ is the following

$$S_{11}(Q,t) = \frac{1}{\Gamma_1 - \Gamma_2}\{[(\Gamma_1 - \Omega_{22})S_{11} + \Omega_{12}S_{21}]e^{-\Gamma_1 t} + [(-\Gamma_2 + \Omega_{22})S_{11} - \Omega_{12}S_{21}]e^{-\Gamma_2 t}\}$$

$$S_{22}(Q,t) = \frac{1}{\Gamma_1 - \Gamma_2}\{[(\Gamma_1 - \Omega_{11})S_{22} + \Omega_{21}S_{12}]e^{-\Gamma_1 t} + [(-\Gamma_2 + \Omega_{11})S_{22} - \Omega_{21}S_{12}]e^{-\Gamma_2 t}\}$$

$$S_{12}(Q,t) = \frac{1}{\Gamma_1 - \Gamma_2}\{[(\Gamma_1 - \Omega_{22})S_{12} + \Omega_{12}S_{22}]e^{-\Gamma_1 t} + [(-\Gamma_2 + \Omega_{22})S_{12} - \Omega_{12}S_{22}]e^{-\Gamma_2 t}\}$$

$$S_{21}(Q,t) = \frac{1}{\Gamma_1 - \Gamma_2}\{[(\Gamma_1 - \Omega_{11})S_{21} + \Omega_{21}S_{11}]e^{-\Gamma_1 t} + [(-\Gamma_2 + \Omega_{11})S_{21} - \Omega_{21}S_{11}]e^{-\Gamma_2 t}\} \qquad (10)$$

For symmetric Ω matrices the solution (10) coincides with the result already given in ref 21. After having given the general solution of eq 5 for an (A–B) block copolymer of arbitrary architecture we now have to calculate specifically the structure factor $\mathbf{S}(Q)$ and the mobility matrix $\mathbf{M}(Q)$ for (A–B) stars.

II.2. The Structure Factor for (A–B) Stars. Recently Benoit and Hadziioannou[9] have developed a general theory that enables one to predict the scattering behavior of multiblock copolymers with various architectures. For starlike (A–B) block copolymers of functionality f they arrive at the following expressions:

$$S_{11}(Q) = fP_\alpha(Q) + f(f-1)A_\alpha(Q)^2$$
$$S_{22}(Q) = fP_\beta(Q) + f(f-1)A_\beta(Q)^2 e^{-2Q^2(R_g^\alpha)^2}$$
$$S_{12}(Q) = S_{21}(Q) = fA_\alpha(Q)A_\beta(Q) + f(f-1)A_\alpha(Q)A_\beta(Q)e^{-Q^2(R_g^\alpha)^2} \qquad (11)$$

Thereby P_α and P_β are the Debye structure factors of the respective blocks

$$A_\alpha = \sum_{i=1}^{N\alpha} \langle \exp(-i\mathbf{Q}\mathbf{r}_{i\alpha})\rangle$$
$$A_\beta = \sum_{j=1}^{N\beta} \langle \exp(-i\mathbf{Q}\mathbf{r}_{j\beta})\rangle \qquad (12)$$

R_g^α is the radius of gyration of the inner block A and N_α and N_β are the respective numbers of monomers.

For a chain with a Flory exponent ν the quantities P and A can be written as

$$P_{\alpha/\beta} \simeq 2N_{\alpha/\beta}^2 \int_0^1 du\,(1-u)\exp(-Q^2(R_g^{\alpha/\beta})^2 u^{2\nu})$$
$$A_{\alpha/\beta} \simeq N_{\alpha/\beta} \int_0^1 du \exp(-Q^2(R_g^{\alpha/\beta})^2 u^{2\nu}) \qquad (13)$$

We note that for the derivation of eq 13 one assumes that independently of the Flory exponent the distance distribution P_{ij} between two arbitrary polymer segments i and j is Gaussian[22]

$$P_{ij}(r_{ij}) = \left(\frac{3}{2\pi\langle r_{ij}^2\rangle}\right)^{3/2} \exp\left(-\frac{3}{2\langle r_{ij}^2\rangle} r_{ij}^2\right) \qquad (14)$$

Furthermore, the screening of the excluded-volume interaction due to the interaction of the different arms of the star is neglected. According to Daoud and Cotton[3] this screening effect leads to blob formation in semidilute polymer solutions with a blob size $\xi(r)$, which increases with the distance from the star center.

Finally, for a Gaussian chain the radii of gyration for the different partial structure factors can be simply expressed by $R_g^{\alpha/\beta}$. Expanding eq 11, we get[8]

$$(R_g^{11})^2 = \frac{3f-2}{f}(R_g^\alpha)^2$$
$$(R_g^{22})^2 = \frac{3f-2}{f}(R_g^\beta)^2 + 6\frac{(f-1)}{f}(R_g^\alpha)^2$$
$$(R_g^{12})^2 = \frac{3}{2}\frac{(3f-2)}{f}(R_g^\alpha)^2 + \frac{3}{2}(R_g^\beta)^2$$
$$R_g^2 = \left(\frac{N^\alpha}{N}\right)^2 (R_g^{11})^2 + \left(\frac{N^\beta}{N}\right)^2 (R_g^{22})^2 + 2\left(\frac{N^\alpha}{N}\right)\left(\frac{N^\beta}{N}\right)(R_g^{12})^2 \qquad (15)$$

II.3. The Mobilility Matrix. In order to evaluate an expression for the generalized mobility we have to consider the dynamics of a polymer in solution, which is governed by the hydrodynamic interactions between different segments. On the basis of the Kirkwood diffusion theory[23] and following the treatment of Akcasu and Gurol[24] and Burchard,[6] the generalized mobility can be

expressed in terms of the Oseen diffusion tensor[6]

$$M_{\alpha\beta}(Q) = \frac{1}{k_B T Q^2}\sum_{jk}\langle \mathbf{Q}\mathbf{D}_{jk}^{\alpha\beta}\mathbf{Q}\exp(-i\mathbf{Q}\mathbf{r}_{jk}^{\alpha\beta})\rangle \quad (16)$$

with

$$\mathbf{D}_{jk}^{\alpha\beta} = \frac{k_B T}{\zeta_j}\delta_{jk}^{\alpha\beta} + (\mathbf{E} - \delta_{jk}^{\alpha\beta})\frac{k_B T}{8\pi\eta_0 \mathbf{r}_{jk}^{\alpha\beta}}\left(\mathbf{E} + \frac{\mathbf{r}_{jk}^{\alpha\beta}\mathbf{r}_{jk}^{\alpha\beta}}{(\mathbf{r}_{jk}^{\alpha\beta})^2}\right)$$

The first term in eq 16 describes the so-called free draining, ζ_j being the monomeric friction coefficient of monomer "j". In dilute solution this contribution is negligible and will be omitted further on. The second term results from the hydrodynamic interaction between monomers j and "k", which is determined by the strength of the back-flow field over the distance $\mathbf{r}_{jk}^{\alpha\beta} = \mathbf{r}_{i\alpha} - \mathbf{r}_{j\beta}$ in the solvent with viscosity η_0. Its contribution to the mobility is given by

$$\phi_{jk}^{\alpha\beta} = \frac{1}{k_B T Q^2}\langle \mathbf{Q}\mathbf{D}_{jk}^{\alpha\beta}\mathbf{Q}\exp(-i\mathbf{Q}\mathbf{r}_{jk})\rangle \quad (17)$$

Due to the tensor character of $\mathbf{D}_{jk}^{\alpha\beta}$ the thermal average in eq 17 leads to bulky expressions. However, Burchard et al.[25] have shown that eq 17 may be approximated to high accuracy by a preaveraged form ϕ_{jk}^{pre} plus a correction term $\Delta\phi_{jk}$:

$$(\phi_{jk}^{\alpha\beta})^{\text{pre}} = \frac{1}{Q^2 k_B T}\langle \mathbf{Q}\mathbf{D}_{jk}^{\alpha\beta}\mathbf{Q}\rangle\langle\exp(-i\mathbf{Q}\mathbf{r}_{jk}^{\alpha\beta})\rangle$$

$$= \frac{1}{6\pi^{3/2}\eta_0 \mathbf{r}_{jk}^{\alpha\beta}}\exp(-Q^2(\mathbf{r}_{jk}^{\alpha\beta})^2)$$

$$\Delta\phi_{jk}^{\alpha\beta} = \frac{Q^2 r_{jk}}{30\pi^{3/2}\eta_0}\exp(-0.72Q^2(\mathbf{r}_{jk}^{\alpha\beta})^2) \quad (18)$$

Again the averaging in eq 18 is performed under the assumption of a Gaussian distance distribution (eq 14). To proceed further[19] we utilize the integral identity

$$\frac{2}{\pi^{1/2}}\int_0^\infty \exp(-S^2(\mathbf{r}_{jk}^{\alpha\beta 2}))\,dS = \frac{1}{\mathbf{r}_{jk}^{\alpha\beta}} \quad (19)$$

and rewrite eq 18 as

$$(\phi_{jk}^{\alpha\beta})^{\text{pre}} = \frac{1}{3\pi^2\eta_0}\int_0^\infty \exp(-(\mathbf{r}_{jk}^{\alpha\beta})^2(Q^2 + S^2))\,dS$$

$$\Delta\phi_{jk}^{\alpha\beta} = \frac{Q^2}{30\pi^2\eta_0}\int_0^\infty \frac{1}{S^2}[\exp(-0.72\mathbf{r}_{jk}^{\alpha\beta})^2Q^2)[1 - \exp[-(\mathbf{r}_{jk}^{\alpha\beta})^2S^2]]\,dS \quad (20)$$

Introducing eq 20 into the expressions for the partial structure factors (eqs 2 and 11) and exchanging summation and integration we finally obtain

$$M_{\alpha\beta}^{\text{pre}} = \frac{1}{3\pi^2\eta_0}\int_0^\infty S_{\alpha\beta}((Q^2 + S^2)^{1/2})\,dS$$

$$\Delta M_{\alpha\beta}(Q) = \frac{Q^2}{30\pi^2\eta_0}\int_0^\infty \frac{1}{\beta_2}[S_{\alpha\beta}((0.72Q^2)^{1/2}) - S_{\alpha\beta}((0.72Q^2 + S^2)^{1/2})]\,dS \quad (21)$$

Equation 21 explicitly shows that in the initial slope approximation the generalized mobility for a polymer with a hydrodynamic interaction is only related to the static structure factor and can be expressed by appropriate integrals over $S_{\alpha\beta}(Q)$. Equation 21 is valid for any polymer conformation as long as one assumes Gaussian distance distribution for the monomer distances $\mathbf{r}_{ij}^{\alpha\beta}$. We will use this relation later on in order to calculate the dynamic response from the measured static structure factors. We call this approach the structural model.

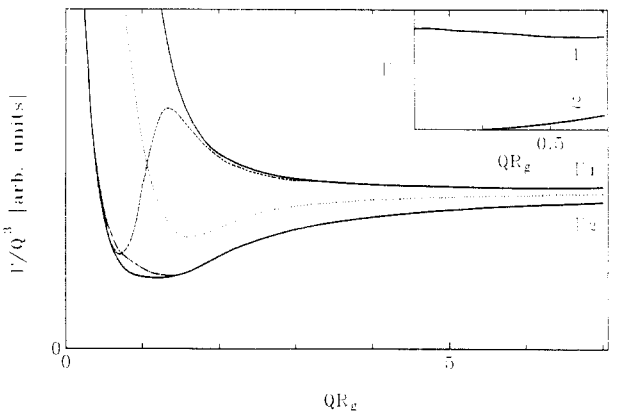

Figure 1. Reduced relaxation rates $\Gamma_{1/2}/Q^3$ for the Gaussian model. The insert presents the rates Γ directly. Note that Γ_1 approaches a constant at low Q. The broken lines give the effective reduced relaxation rates for various contrast conditions: dashed line, shell contrast; dashed dotted line, core contrast; dotted line, average contrast.

II.4. Results for Gaussian Stars. In order to demonstrate the Q dependence of the relaxation rates and their respective spectral weights, we have calculated them according to eqs 3 and 11 for Gaussian stars assuming three different contrasts: (i) core contrast ($a_1 = 1$; $a_2 = 0$), (ii) shell contrast ($a_1 = 0$, $a_2 = 1$), and (iii) average contrast ($a_1 = -a_2$). In addition we have determined the $1/e$ decays or effective relaxation rates Ω for the respective cross sections. For $N_1 = N_2$ and $f = 12$, Figure 1 displays the reduced relaxation rates Γ_i/Q^3 as a function of QR_g. Figure 1 also shows the reduced effective relaxation rates Ω/Q^3 for the three different contrasts. Γ_2/Q^3 exhibits a minimum around $QR_g \sim 1$ and at low Q describes the translational diffusion of the whole star. This can be seen from the insert of Figure 1, which displays the nonreduced eigenvalues versus QR_g. At low QR_g, Γ_2 increases proportional to Q^2 thus exhibiting diffusive behavior. On the other hand Γ_1 reaches a finite value at low Q. It corresponds to an "optic"-like mode and describes the relative motion of the star shell with respect to the core. We note that similar behavior has already been predicted for a linear diblock copolymer.[21] At higher QR_g the minimum in Γ_2/Q^3 is absent and finally in the high QR_g limit both modes converge, describing the Zimm relaxation of the arms. Figure 2 represents the spectral weights of the two eigenvalues under different contrasts. We find that (i) for the core contrast in a scattering experiment basically the eigenmode Γ_2 is observed. Some small deviations occur around $QR_g \sim 1$ where the dashed dotted line in Figure 1 displaying the corresponding effective relaxation rates lies above the curve for Γ_2/Q^3. Regarding the spectral weights we observe that around this Q value a slight admixture of Γ_1 is present; (ii) for shell contrast we observe a crossover in the spectral weight from Γ_2 below $QR_g \sim 1$ to Γ_1 above this value. This gives rise to a maximum of the effective reduced rate Ω/Q^3 at $QR_g = 1.35$. Finally, (iii) under average contrast conditions at low QR_g the scattering experiment probes the optic-like mode Γ_1 while toward higher QR_g both eigenvalues contribute significantly to the effective rate (see Figure 2c). We note, however, that at average contrast conditions the scattering decreases to zero for Q approaching zero. Therefore in practice the optic mode may not be observable at low Q.

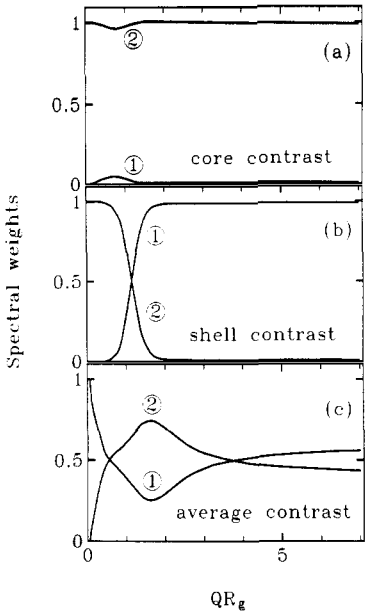

Figure 2. Spectral contributions of the two modes and Γ_1 (1) and Γ_2 (2) to the intermediate scattering function for different contrast conditions.

Recently, Burchard et al.[8] calculated initial slopes for diblock copolymer stars under different contrast conditions. They report different apparent diffusion coefficients depending on the applied contrast. According to our calculations these initial slope results are affected by very small admixtures of the optic-like mode Γ_2, which at low QR_g is many orders of magnitude faster than the diffusive mode. In the mathematical $t \to 0$ limit it therefore changes the initial slope even at an infinitesimal spectral weight. Experimentally, however, this effect is irrelevant and the observable relaxation rates always reflect the true translational diffusion of the molecule. Finally, we relate the outcome of this Gaussian model to our earlier observed apparent renormalization of the reduced relaxation rate with $Q^2S(Q)$.[14] From eq 7 we have $\Omega/Q^3 = Q^2M(Q)/(Q^3\mathbf{S}(Q))$. In the Zimm regime the Q dependence of the mobility is given by $M(Q) \sim 1/Q$. This results in

$$\Omega/Q^3 \simeq \text{const}/Q^2\mathbf{S}(Q) \qquad (22)$$

At low Q, however, when deviations from $M(Q) \sim 1/Q$ occur—$M(Q)$ becomes a constant for Q approaching zero—eq 22 is no longer valid.

III. Experimental Section

For our study of the relation between the structure and dynamics of star molecules, we choose 12-arm polyisoprene stars, which have proved themselves to be well suited for static and dynamic investigations involving neutron scattering.[14] Three different samples were prepared (Table I): the sample 12PD was a star consisting of diblock copolymers, half deuterated, half protonated, each block having a molecular weight of 4000. They were attached to the center seed molecule in such a way that the star core was protonated. In sample 12DP the labeling was reversed. Sample 12P was a fully protonated 12-arm star with a molecular weight of 8000/arm (sample 12-IV of ref 26).

The synthesis procedures used to prepare the isotopically labeled diblock stars were essentially those described elsewhere.[27-29] The initiator was purified *tert*-butyllithium[30] (Lithium Corp. of America), while the linking agent was the dodeca chlorosilane previously used.[27] The isoprene-h_8 was obtained from Wiley Organics and the d_8 counterpart from Cambridge Isotope and Merck, Sharp and Dohm.

The diblock polyisoprene (d_8–h_8 and h_8–d_8) were prepared in a 30/70 (v/v) benzene/cyclohexane mixture at 20 °C. The polymerization conditions used led to a statistically uniform stereoirregular chain microstructure (~5% 3,4; ~75% cis 1,4; ~20% trans 1,4). After the completion of the polymerization of the initial isoprene segment a small amount (~1 cm^3) was removed for evaluation via size exclusion chromatography. This procedure was repeated after the diblock was prepared. The size exclusion chromatography evaluation of the initial segments of the respective diblocks and the diblock copolymers yielded M_n/M_w and M_w/M_n ratios of 1.06 or less. No corrections for column broadening were made. The diblocks had a molecular weight M_w = 8000.

The linking agent was added and the solution kept at 25 °C for 1 week. After fractionation to remove unlinked arms, the branch-point functionality was determined by osmometry measurements on the diblock arm and the star. We found functionalities of f = 11.9 (d_8–h_8) and f = 11.7 (h_8–d_8). Supplementary low-angle laser light scattering measurements on the star yielded M_w/M_n ratios for the stars of less than 1.04; findings that were fortified via size exclusion chromatography (Figure 3).

In order to achieve core, shell, or full contrasts the samples 12PD, 12DP, and 12P were dissolved in deuterated *n*-octane. The resulting contrast factors for S_{11}, S_{12}, and S_{22}, respectively, are displayed in Table I. In order to achieve average contrast a mixture of partially deuterated toluene molecules was used. This mixture had the advantage that the small angle scattering from the solvent was very low. Using a corresponding mixture of deuterated and protonated octanes leads to a significantly higher coherent scattering in the Q range of interest. For the small-angle scattering experiments, solutions of 1%, 2%, and 4% monomer concentration were prepared. The neutron spin–echo experiments were carried out at 4% concentration.

IV. Small-Angle Neutron Scattering Experiments

Small-angle neutron scattering (SANS) experiments were performed by using the small-angle camera D17 at the Institut Laue-Langevin (ILL) in Grenoble. We utilized a neutron wavelength λ = 10.2 Å with 10% monochromatization. The multidetector was positioned at a distance of 2.85 m from the sample and placed at the two mean scattering angles of 4.5° and 14.5° offering a Q range 7×10^{-3} Å^{-1} < Q < 0.2 Å^{-1}. The measurements were carried out at room temperature. We investigated the partially labeled 12-arm polyisoprene stars under three different contrast conditions (see Table I): Sample 1 mainly revealed the scattering from the star core, sample 2 allowed the observation of the star shell, and sample 3, which was close to a mean scattering contrast of zero, was sensitive to the interference term S_{12} of the structure factor. Furthermore, we studied a fully labeled 12-arm star of the same size (sample 4). In order to control interstar interaction effects we studied three different monomer concentrations (1%, 2%, and 4%). The data were corrected for the solvent scattering and the estimated incoherent scattering contribution from the dissolved polymer. Thereafter they were normalized to a water standard. Below Q = 0.04 Å^{-1} the scattering patterns were found to depend on the monomer concentration. There, by using the usual Zimm plots, the intensities $I(Q)$ were extrapolated to zero concentration. These intensity values are considered further on. Figure 4 presents the corrected data for the three different scattering contrasts in a generalized Kratky representation. Since the solvents used are good solvents for PI, we expect swollen chain conformations and therefore plot $I(Q)Q^{5/3}$ versus Q. The solid lines represent the result of fits to the neutron cross sections of the eqs 3 and 11–13. Thereby the appropriate contrast factors according to Table I were used. In general we performed the fits using the Flory exponents ν = 0.5 (Gaussian coil) and ν = 0.6 (swollen coil). The fitting range was restricted to the low-Q regime

Table I
Star Polymer Samples Used in the Scattering Experiments[a]

sample	polymer	M_w	solvent	η_o, cP	a^2_{11}, b	$a_{11}a_{22}$, b	a^2_{22}, b
1	12 PD	9.6×10^4	octane-*d*	0.386	0.92	−6.83	50.1
2	12 DP	9.6×10^4	octane-*d*	0.386	50.1	−6.83	0.92
3	12 DP	9.6×10^4	90.4% $C_7D_5H_3$ 9.6% $C_7D_3H_5$	0.42	15.5	−16.3	17.2
4	12 P	9.6×10^4	octane-*d*	0.386	50.1		

[a] a_{11} and a_{22} are the scattering length densities for the star core and the star shell, respectively. b denotes barn. 1 barn = 10^{-24} cm^2.

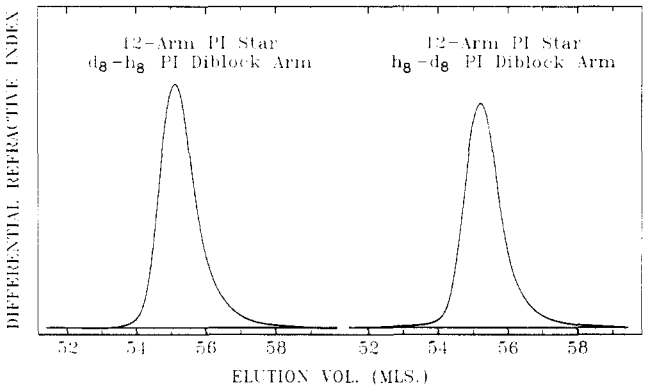

Figure 3. Results of size exclusion chromatography for the two diblock copolymer stars.

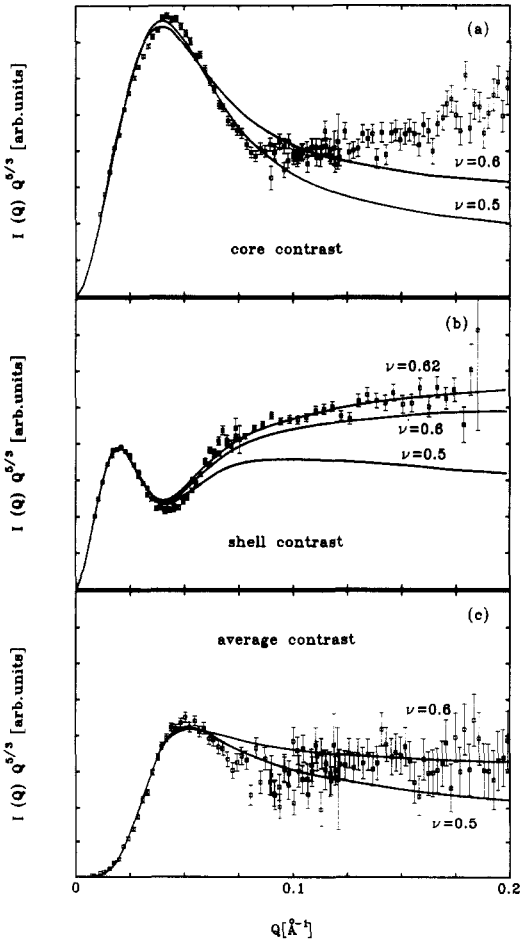

Figure 4. SANS data from the diblock copolymer stars under three contrast conditions in a generalized Kratky representation. The solid lines are the result of a fit with the Gaussian and swollen star model of section II. The indices ν indicate the Flory exponent: (a) sample 1; (b) sample 2; (c) sample 3 (see Table I).

($Q < 0.075$ Å^{-1} for core and average contrast and $Q < 0.05$ Å^{-1} for shell contrast). The fits revealed the respective block lengths $R_g^{\alpha,\beta}$, from which following eq 15 the radii of gyration may be calculated. Table II presents the results for $\nu = 0.5$ and compares the thus-calculated R_g values with those obtained from the Guinier regime.

Table II
Radii of Gyration Obtained for the Different Samples and Partial Structure Factors in Various Approaches[a]

partial struct factor	R_g (Guinier), Å	R_g (calcd), Å	sample (contrast)	R_g (Guinier), Å	$R_g^{\alpha/\beta}$, Å
S_{11}	49.7 ± 1	50	core	47 ± 2	29.7
S_{22}	78 ± 1	83.8	shell	80 ± 2	27.7
S_{12}	76 ± 2	70	average		33
S	70[b]	69.5[c]	fully labeled star	69 ± 2	

[a] R_g (Guinier) is the radius of (column 2, from the partial structure factors; column 5 from the measured data) gyration obtained in the Guinier regime. $R_g^{\alpha/\beta}$ are the radii of gyration for copolymer blocks obtained from the Gaussian fits. R_g (calcd) denotes the radius of gyration evaluated on the basis of $R_g^{\alpha/\beta}$ in the framework of the Gaussian model. [b] This value has been calculated on the basis of the measured R_g for the partial structure factors. [c] This result comes from the Gaussian fit of the full structure factor.

Other than for linear polymers the static cross section in the Kratky representation exhibits pronounced structure in the Q range around $QR_g \sim 1$. With core contrast (Figure 4a) we observe a strong peak, which already has been reported for fully labeled stars.[14,15] As was seen for a fully labeled star,[14] we find for the star core that in this peak region the Gaussian model reproduces the structure quite well while the excluded-volume model predicts a more diffuse peak. Furthermore, the radius of gyration derived from a fit with the Gaussian model agrees well with that obtained from the Guinier regime (Table II). At higher Q, however, where the cross section reveals the asymptotic power law behavior, $I(Q) \sim Q^{-1/\nu}$, the Gaussian model clearly fails. We note, that already on fully labeled stars in Θ solvents similar deviations have been observed.[31] Therefore, it is not astonishing that also the swollen chain configuration does not sufficiently take into account the chain stretching present in the star core. A power law fit for $Q > 0.1$ Å^{-1} reveals $S(Q) \sim Q^{-1.4}$, corresponding to a Flory exponent $\nu \simeq 0.71$. However, as already indicated by the theoretical cross section for $\nu = 0.6$, which still decreases in the considered Q range and does not yet reach the asymptotic plateau level, the scattering pattern still contains interarm interference effects and does not reveal the single-arm statistics. Nevertheless, qualitatively, we may state that the inner star is an object with a rather well-defined boundary (sharp structure at low Q) containing considerably stretched polymer chains.

With shell contrast (Figure 4b) the scattering pattern in the Kratky representation is characterized by a low-Q peak followed by an intermediate minimum, which toward higher Q is succeeded by an elevated plateau level. Again the peak structure is best reproduced by the Gaussian model, which also provides good internal consistency with respect to radius of gyration (Table II). On the other hand, at high Q, it disagrees strongly with the experi-

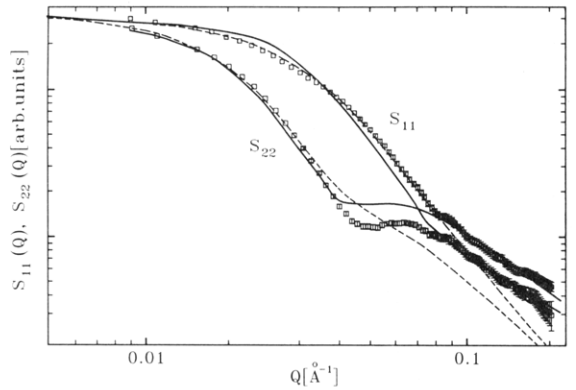

Figure 5. Partial static structure factors S_{11} and S_{22}. The dashed lines represent the fit with the Gaussian model. The solid lines are the results of the molecular dynamics simulation for a 10-arm 50 segment per arm star of ref 7.

mental data. The swollen chain model provides a reasonably good description of the full scattering pattern. If, in addition, we allow for a variation of the Flory exponent and perform a fit over the full Q range, for $\nu = 0.62$ we obtain a good fit over the full Q range, the only systematic deviations occurring in the region of the intermediate minimum. An exponent $\nu = 0.62$ corresponds to a slightly more stretched chain conformation than in the swollen state ($S(QR_g \gg 1) \sim Q^{-1.61}$ instead of $\sim Q^{-5/3}$).

Finally, Figure 4c presents the data taken under average contrast conditions. As for the other two results the low-Q structure is better represented by the Gaussian model while the asymptotic high-Q behavior agrees better with the swollen star model. However, since under average contrast conditions the scattering is very weak, the data at high Q are affected by considerable error bars thereby limiting their significance.

In the next step of data evaluation, from the three different contrasts we extracted the partial structure factors S_{11}, S_{22}, and S_{12}. In order to reduce the effect of statistical noise, the data were smoothed by fitting a thirdorder polynominal to the respective seven points around the considered data point. Then the appropriate system of linear equations was solved, revealing the partial structure factors for each Q value. Figure 5 shows S_{11} and S_{12} in double-logarithmic representation. The solid lines display the result of a molecular dynamics simulation[7] for a 10-functional star with 50 segments per arm, while the dashed lines reproduce the Gaussian model discussed above. Qualitatively, the MD simulation result exhibits the essential features of the experimental data. In particular the intermediate intensity plateau of S_{22} is well reproduced; also the slightly different asymptotic Q dependences of the two structure factors are predicted. In comparison the Gaussian model (dashed lines) is virtually featureless. However, quantitatively, the MD calculations and the experiment differ considerably. Most importantly this concerns the step height of the steep low-Q increse of the partial structure factors. While the experimental data exhibit about the same step height for both S_{11} and S_{22}, the MD simulation predicts a larger step for S_{11} leading to an inverse sequence of the intensity curves at high Q. Furthermore, the intermediate plateau region of S_{22} is more narrow than predicted.

Figure 6 displays our result for the interference term S_{12} again in a double-logarithmic plot. Since in the Q region $0.045 < Q < 0.06$ Å^{-1} S_{12} becomes negative we show $|S_{12}|$. The solid line reproduces the prediction of the Gaussian model—MD simulations for this quantity are not available. Again, we note that the experimental

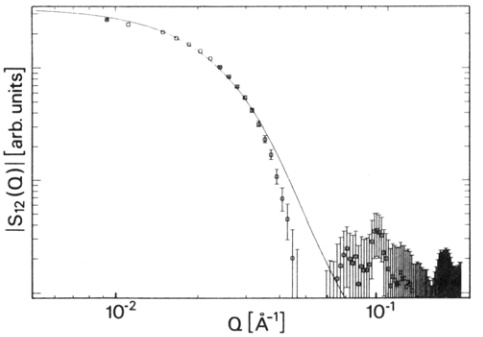

Figure 6. Partial structure factor S_{12}. The solid line is a result of the Gaussian model.

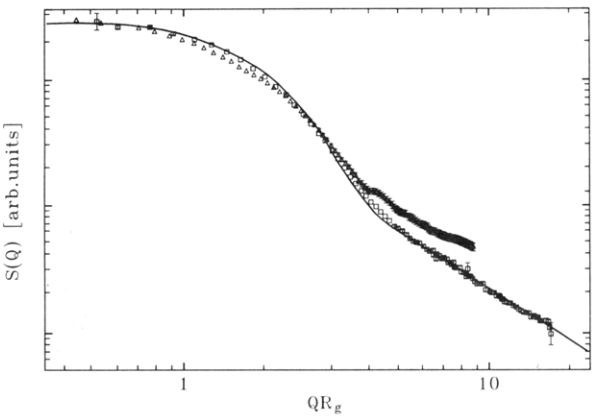

Figure 7. Structure factor of the fully labeled star (sample 4) (□). The solid line displays the result of the molecular dynamic simulation for the 10-arm 50 segment per arm star of ref 7. The triangles represent the result for S_{11}. Note that at high QR_g deviations from scaling are evident.

data exhibit considerably more structure than the model. The well-defined minimum at intermediate Q—there S_{12} becomes negative—indicates a well-developed core–shell structure of the star.

The radii of gyration for the three partial structure factors evaluated from the Guinier regime are given in Table II and are compared with the R_g values calculated according to eq 15 from the Gaussian fits of the star data (see above). While for S_{11} and S_{22}, good agreement is achieved, the Guinier value for R_g from S_{12} is significantly larger than the value calculated in the framework of the Gaussian model. This discrepancy is another signature of the pronounced *core–shell structure*, which is not present in the Gaussian model.

Finally, Figure 7 compares the structure factor obtained from the fully labeled 12-arm star (sample 4, Table I) with the result of the MD simulation of a correspondingly labeled 10-arm 50-segment per arm star.[7] We find nearly perfect agreement. The radius of gyration of this star has been determined in the Guinier range (Table II). As it should be, its value is smaller than that of the star shell and it agrees very well with the expected value of R_g calculated on the basis of the results for the partial structure factors from eq 15. The structure factors of eqs 11–14 and a detailed scaling analysis[3] predict that the scattering pattern of stars with different molecular weight but the same functionality should scale with the radius of gyration. In Figure 7 we compare the scattering patterns from the fully labeled star with S_{11}, the structure factor of the star core in scaling them with the appropriate R_g's. Unexpectedly the data sets do snot match but deviate at higher Q. The step height between the low-Q plateau and the asymptotic high-Q tail is differ-

ent for the two cross sections. In addition the asymptotic Q dependences deviate from each other ($S_{11}(Q) \sim Q^{-1.40}$, $S(Q)$ (fully labeled) $\sim Q^{-1.54}$), indicating the more stretched chains close to the star center. While the second result is not unexpected, the first may pose some questions on the scaling approach. There the star is treated in analogy to a semidilute solution of linear polymers with a blob structure describing the screening of the excluded-volume interaction. Other than in semidilute solutions where the blob size ξ depends only on the polymer concentration, in the case of stars it increases with the distance from the star center. The largest blobs situated at the periphery of the star, thereby, contain most of the chain segments. Their size scales as $\xi \sim R_g f^{-1/2}$. Neglecting the high-density meltlike zone close to the star center, which is only important for stars of very high functionality, we may distinguish three scaling regimes for the scattering function: (i) At low Q we have the Guinier regime where the total scattering from one star is given by $S(Q) \simeq (Nf)^2(1 - (1/3)Q^2R_g^2)$. (ii) At high Q we are in the asymptotic regime where we observe an incoherent superposition of the coherent scattering originating from the polymers in each blob. At the onset of this regime the intensity may be expressed as $n_b(\xi/\sigma)^{2/\nu}$, where $n_b = (R_g/\xi)^3$ is the number of blobs, $(\xi/\sigma)^{1/\nu}$ gives the number of segments per blob, and σ is the segment length. (iii) In the intermediate regime the intensity has to drop from the low-Q plateau to the high-Q asymptotic level. The magnitude of this intensity drop is $[(R/\xi)^3(\xi/\sigma)^{1/\nu}]^2/(R/\xi)^3(\xi/\sigma)^{2/\nu} \sim f^{3/2}$, independent of ν and the number of segments per arm. It is this relationship that appears to be at variance with our result. We note further that other than the SANS results the MD simulations for S_{11} and the corresponding full star follow the scaling relationship. Thus the discrepancies between the MD calculations and S_{11} and S_{22} in Figure 5 bring about the deviations from scaling.

V. Neutron Spin-Echo Experiments

In order to evaluate the relaxation dynamics of the star molecules we performed neutron spin-echo (NSE) experiments on the same samples that were studied by SANS. In a NSE measurement the velocity change of the neutron due to inelastic scattering events is determined directly via the difference in the number of Larmor precessions of the neutron spin in identical magnetic guide fields before and after the sample.[32] NSE is a Fourier method and essentially measures the real part of the normalized intermediate scattering function $S(Q,t)/S(Q,0)$. The Fourier time, thereby, is proportional to the applied guide field H. A spin-echo scan is performed by varying the guide field and thereby studying the intermediate scattering function at different Fourier times.

Our experiments were carried out by using the NSE spectrometer IN11 at the ILL. The nominal neutron wavelength was $\lambda = 8.56$ Å with $\Delta\lambda/\lambda \sim 20\%$. The experiments covered a Q range 0.026 Å$^{-1} < Q < 0.128$ Å^{-1} and accessed Fourier times 0.3 ns $< t <$ 16.1 ns. The achieved energy resolution was $\Delta E \sim 20$ neV taken from the $1/e$ decay of the scattering pattern from a glassy PSD/PSH standard. We measured at a temperature $T = 50$ °C using polymer solutions of generally 4% monomer concentration. The data were corrected for the background measured on the respective pure solvents and for the energy resolution of the instrument. We note that the resolution correction in Fourier time space is performed by simple division and does not involve deconvolution procedures. Therefore, model-independent investigations of spectral line shapes become possible. In an exemplary way, Figure 8 presents neutron spin-echo data from sample 2 (Table I), providing shell contrast. The data are plotted logarithmically versus the Fourier time, the parameter being the momentum transfer Q. With increasing Q we observe a strong increase of the star relaxation rate. Furthermore, we realize significant deviations from single-exponential decay, which in Figure 8 would show itself by straight lines.

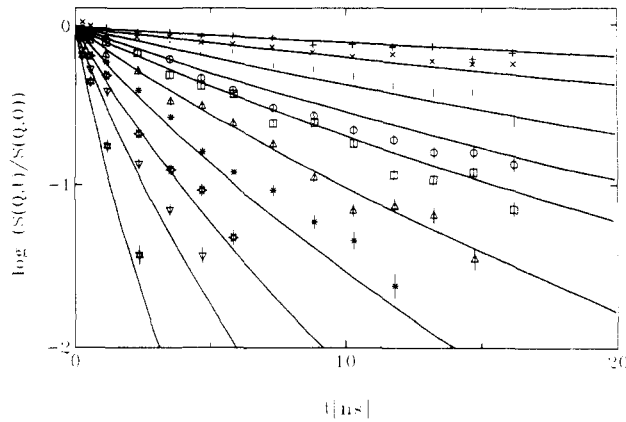

Figure 8. Neutron spin-echo spectra obtained for the star with shell contrast (sample 2). The solid lines are the result of a fit with the structural model to the spectra using only data points for the first 4 ns. The data represent the following Q values: (+) $Q = 0.026$ Å^{-1}; (×) $Q = 0.032$ Å^{-1}; (|) $Q = 0.038$ Å^{-1}; (○) $Q = 0.045$ Å^{-1}; (□) $Q = 0.051$ Å^{-1}; (△) $Q = 0.064$ Å^{-1}; (*) $Q = 0.076$ Å^{-1}; (☆) $Q = 0.089$ Å^{-1}; (▽) $Q = 0.102$ Å^{-1}; (☆) $Q = 0.127$ Å^{-1}.

The theoretical considerations developed in section II are concerned with the short-time relaxation behavior of the initial slope of the relaxation function. Deviations from the initial relaxation could in principle be treated by introducing memory terms to the equation of motion;[11] an approach that leads to considerable mathematical complication. For our data evaluation we chose an approximation that accounts for the deviations from the initial slope behavior. Already in earlier experiments[14,17] we found that the dynamic structure factor $P_{DG}(Q,t)$ of a Zimm chain (which was derived by Dubois Violette and de Gennes[33] for a polymer chain in dilute solution) describes the line shape of the star relaxation spectra. Consequently, we fitted the experimental spectra with $P_{DG}(Q,t)/P_{DG}(Q,0)$. The fit was restricted to the short-time behavior $t < 4$ ns where deviations from the Zimm line shape were not observable. At longer times, in particular for the star core, strong deviations become evident and will be discussed later on. At each Q value these fits revealed characteristic relaxation rates Ω. Figures 9, 10, and 11 present these results for the star shell and core, the average contrast, and the fully labeled star, respectively. In these figures we present the reduced relaxation rates, Ω/Q^3, which are most appropriate to display relaxation phenomena in the presence of a hydrodynamic interaction (see also introduction).

Since the data were taken at relatively high monomer concentration (4%) as is evident from the SANS data, below $Q < 0.04$, interaction effects between different star molecules come into play and we start to observe elements of the collective response of the star ensemble. In terms of the usual de Gennes narrowing approach, this interstar relaxation modifies the observed relaxation rates by[8]

$$\Omega_{obs} = \Omega/\tilde{S}(Q) \tag{23}$$

The intrinsic rate Ω is obtained from the observed rate by multiplying with $\tilde{S}(Q)$, the interstar structure factor.

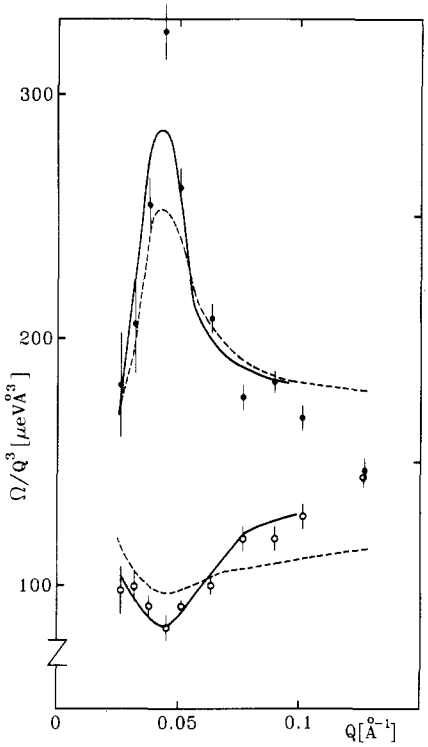

Figure 9. Reduced effective relaxation rates from a fit of the initial decay of the experimental spectra to the Zimm dynamic structure factor: (●) shell contrast; (○) core contrast. The dashed lines represent the Gaussian model; the solid lines are the results from the structural model.

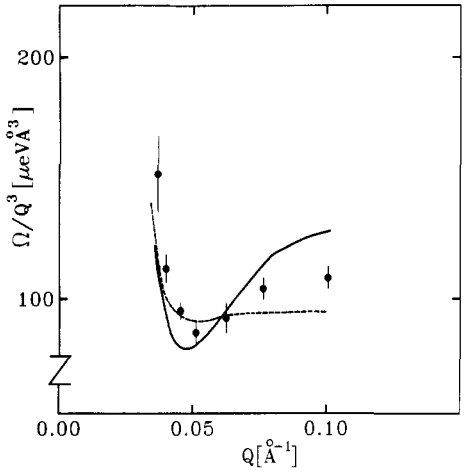

Figure 10. Reduced effective initial relaxation rates of the experimental spectra taken under average contrast conditions: solid line, structural model; dashed line, Gaussian model.

$\tilde{S}(Q)$ is obtained by dividing the SANS results at 4% monomer concentration by the $c = 0$ extrapolated single star structure factor. $S(Q)$ was found to be identical for all the labelings, implying that it has the same effect on all the partial structure factors. This justifies eq 23 for our concentration range. At the Q values of the dynamic experiments these corrections amount to $Q = 0.026$ Å^{-1}, $\tilde{S}(Q) = 0.66$; $Q = 0.032$ Å^{-1}, $\tilde{S}(Q) = 0.80$; and $Q = 0.038$ Å^{-1}, $S(Q) = 0.91$. The low-Q relaxation rates displayed in Figures 9–11 have been corrected accordingly.

A comparison with the theoretical models of section II has been made for two cases: (i) in a first approach we took Gaussian partial structure factors where the values for the radii of gyration of the two blocks were taken from the evaluation of the SANS data (Table II); (ii) second, in the framework of the generalized mobility matrix, which may be evaluated for any arbitrary structure factor (eq 21), we calculated the dynamic response on the basis of the experimentally determined partial structure factors. Both models were fitted to the experimental relaxation curves, again considering only the short time behavior ($t \leq 4$ ns). In order to approximately take into account the experimental line shape, the two exponential relaxation terms in eq 10 $\exp(-\Gamma_{1/2}t)$ were replaced by normalized Zimm dynamic structure factors $P_{DG}(Q,t)/P_{DG}(Q,0)$. Their initial slopes were set to Γ_1 and Γ_2, respectively. At low Q the interaction correction of eq 23 was employed. For each set of spectra taken at a given contrast the only fitting parameter was the time scale of relaxation, which according to eqs 7 and 21 is measured in units of T/η_0. Table III presents the results for T/η_0 derived from the various fits. In Figures 9–11 the dashed lines present the predictions of the Gaussian model while the solid lines describe the dynamic response calculated on the basis of the observed structure factors. In order to arrive at these curves, which are to be compared with the results of fitting the experimental data to $P_{DG}(Q,t)$, we have assumed the following scheme: starting from the fitted relaxation rates, according to the modified eq 10 (replacement of $\exp(-\Gamma_{1/2}t)$ by $P_{DG}(Q,t)$) we have reconstructed theoretical relaxation spectra at time values coinciding with the experimental ones. These theoretical spectra were fitted with $P_{DG}(Q,t)$. The resulting Q-dependent relaxation rates are the basis for the theoretical curves in the above figures.

The Gaussian model (dashed lines) qualitatively displays the general features of the experimental results but the agreement with the experimental relaxation rates is

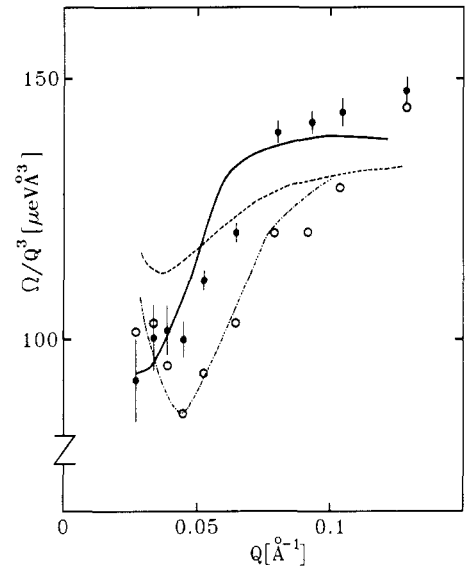

Figure 11. Reduced effective initial relaxation rates for the fully labeled star (●) compared with those from the star core (○): solid line, structural model; dashed line, Gaussian model for the fully labeled star. The dashed dotted line gives the prediction of the structural model for the star core.

Table III
Parameter T/η_0, Which Sets the Time Scale for the Relaxation Process, As Obtained from the Fits with Gaussian and the Structural Model

sample	T/η_0, K cP^{-1}, Gaussian model	T/η_0, K cP^{-1}, structural model
1. star core	410 ± 9	324 ± 6
2. star shell	658 ± 14	474 ● 13
3. average cont[a]	408 ± 15	280 ● 4
4. full star	525 ± 10	389 ± 7

[a] The parameter T/η_0 obtained at average contrast has been corrected for the ratio of viscosities of octane and toluene.

poor. Overall the predictions of the Gaussian model exhibit less pronounced structure than actually observed, e.g. for shell and core contrast in Figure 9 we observe that both the peak and the minimum in the reduced relaxation rates are predicted at the correct position in Q. However, both of them are much weaker than measured experimentally. Similar observations hold also for the cases of average and full contrast (Figures 10 and 11). Compared to the Gaussian model the structural model provides a superior picture. The agreement with respect to the Q dependence of the characteristic frequencies is nearly quantitative. In particular both the minimum as well as the maximum of Ω/Q^3 for core and shell relaxation are very well reproduced (Figure 9). Thus, the relaxation data are well described in terms of the two-mode picture of the RPA model: For Q values above the maximum the shell relaxation mode may be identified with the "optic" relaxation mode explained in section II. Toward lower Q the "acoustic" diffusive mode gains spectral weight and we observe the down swing of Ω/Q^3 at low Q. On the other hand the core relaxation behavior reflects nearly exclusively the low-lying second acoustic-like star relaxation mode, which undergoes a minimum where the shell relaxation arrives at the maximum. For average contrast conditions the RPA model predicts a strong low-Q increase of the reduced relaxation rate, since there the optical mode Γ_1 gains weights. This behavior is seen in Figure 10 where below $Q = 0.05$ Å^{-1} the data display the predicted behavior. Since at average contrast the scattering signal approached zero at $Q = 0$, we were not able to follow this mode toward the lowest Q values. Figure 11 compares the relaxation behavior of the fully labeled star with that of the core. We find that the high-Q flank of the star relaxation minimum is shifted toward lower Q values. In terms of the RPA model this shift is explained by an admixture of the "optical" shell mode to the relaxation spectrum causing faster effective relaxation at intermediate Q values. Finally, going back to the SANS data (Figures 5 and 6) we note that in the Q region, where the observed cross sections exhibit the most structure, the Gaussian model deviates most strongly. It is the same Q range where the dynamic data display their pronounced features. Thus, the observation that the structural model describes the relaxation data much better than the Gaussian model is another manifestation of the predicted intimate relation between structure and dynamic response.

While it is evident that the Q dependence of the short-time star relaxation can be exclusively explained on the basis of the star structure, the time scale of these relaxations does not fit into this simple picture. In the model of hydrodynamic interaction used in section II this time scale is solely determined by the temperature divided by the viscosity of the solvent T/η_0. For our experiment this number is 837 K/cP. The results of the fitting process are below this theoretical value, and furthermore they also differ considerably for the different partial structure factors.

Concerning the magnitude of the time scale of relaxation, the difference between the Gaussian and the structural model originates from the different chain statistics used.[34] Depending on these statistics for asymptotic high-Q values the integrals of eq 21 differ by 30% between Gaussian and swollen chains, accounting for the difference between the two results. Comparing the result for the less constrained star shell with the theoretical expectation, we find a ratio of 1.77, which is of the same order as what has been obsrved for linear PDMS molecules in good solvents.[35] The origin of this deviation is not well understood but must be related to details of the interaction between polymer and solvent.

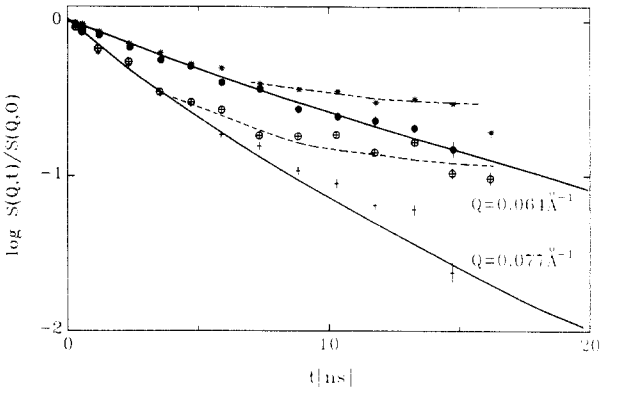

Figure 12. Relaxation spectra of the fully labeled star (●, +) and the star core (*, ⊕) at two different Q values. The solid lines represent the result of a fit of the Zimm dynamic structure factor to the initial relaxation of the fully labeled star. The dashed lines are guides to the eye showing the retardation of the relaxation for the star core.

For undisturbed hydrodynamic interactions the outcome for the time scale of relaxation should have been identical for all dynamic structure factors (each row in Table III). Instead we find a faster time scale for the shell compared to the core with the fully labelled star somewhere in between. Considering the progressive screening of the hydrodynamic interaction as the star center is approached, qualitatively this result is not unexpected. However, quantitatively a calculation of this effect is very difficult. In the calculations of section II the problem of screening was omitted completely. Its consideration implies that the integral relationship between the static structure factor $S(Q)$ and the generalized mobility $M(Q)$ (eq 21) is lost—the hydrodynamic screening length as an intrinsically dynamic length scale that for a star depends on the distance from the star center cannot be infered from static data alone. Nevertheless our experiment shows that we may distinguish between structural effects, which determine the Q dependence of the various relaxation rates, and additional dynamic effects, which are accounted for by varying time scales of relaxation for the different partial structure factors.

The theoretical approach described in this paper dealt with the short-time dynamic response of the star molecules. Consequently, up to now we only discussed the experimental short-time relaxation behavior. As can be seen in Figure 8, by using the Zimm dynamic structure factor an extrapolation of the thus determined relaxation spectra toward longer times remains a good description for the experimental data of the outer star. Similar observations are also made for the fully labeled star, while the long-time relaxation of the star core seems to be strongly retarded. Figure 12 demonstrates this behavior, showing a comparison between the relaxation spectra obtained at two different Q values for the fully labeled star and the star core. At short times ($t \leq 4$ ns) both sets of spectra nearly agree—the data points for the full star are found slightly below the values for the star core. At longer times, however, both sets of spectra disagree strongly. While the data points from the fully labeled star follow the extrapolated Zimm structure factor (solid lines), the relaxation behavior of the star core seems to reach a plateau level at longer times.

It is tempting to explain the observed retardation process of the core relaxation with interarm entanglements

as recently proposed on the basis of scaling arguments.[36] In the simplest Daoud–Cotton picture each arm of a star should extend from the center into a cone with an opening angle $\sim f^{-1/2}$. These cones are filled with blobs of size $\xi(r) \sim rf^{-1/2}$. If a blob performs an angular displacement of order $f^{1/2}$, it will fall into an adjacent cone leading to entanglements between adjacent arms. In order to relax an arm conformation completely, starting from the outer rim, all such entanglements have to be disentangled. This process leads to an exponential dependence of the disentanglement time τ_e on $f^{1/2}$. Thus, compared to normal Zimm relaxation with increasing functionality the according relaxation process is slowed down strongly.

In the scattering function this process should be visible in the pairwise correlation of different arms. Though a precise calculation has not yet been performed, one may argue that such entanglement-caused retardation effects should be visible best in the arm pair correlation function close to the star center—for complete relaxation the outer part has first to disentangle. On the other hand, looking at the full star, these disentanglement processes are likely to be obscured by the motion within the outer blobs containing most of the segments. A definite proof of this interpretation could, e.g., be obtained, if one compares the relaxation of the star core with that of a core-size small star that is not subject to the outer entanglements.

VI. Summary and Conclusion

This work investigated the relationship between polymer architecture and its dynamic response. On the basis of an RPA approach, we calculated the partial static and dynamic structure factors for polymer stars with core shell contrast. The dynamic response was evaluated for the first cumulant. In Gaussian approximation we explicitly calculated the two Q-dependent relaxation rates of the inner and outer star resembling acoustic- and optic-like modes. Furthermore, we pointed out a general relation between the structure and dynamics of star with arbitrary arm statistics.

Summarizing the SANS results, we have measured the partial and full structure factors of a 12-arm star with shell–core contrast and a fully labeled star, respectively. The pertinent experimental results are the following: (i) At low Q the data are reasonably well described in terms of the Gaussian star model. The radii of gyration measured in the Guinier regime, thereby, agree with those obtained from the Gaussian fits. The expected relationships between the different R_g's are well fulfilled. (ii) In the asymptotic high-Q regime, we find Flory exponents indicating stretched arm configurations. The arm stretching is more pronounced for the core than for the shell. (iii) The star cross sections exhibit pronounced structure at intermediate Q values, which is reproduced neither by the Gaussian nor by the simple swollen star model. It must originate from a well-defined core-shell structure. Recent MD simulations are in good qualitative agreement with the experimental partial structure factors and in practically quantitative agreement with the result for the fully labeled star. (iv) Scaling the results for the star core to those of the fully labeled star yields deviations from the expected scaling of the structure factors.

Using the same samples as in the SANS experiments, the dynamic partial and full structure factors were investigated on the NSE spectrometer. In the intermediate Q range ($QR_g > 1$) where anomalies in the static data are prominent, the dynamic data for short-time relaxation exhibit strong deviations from the normal $\Omega \sim Q^3$ Zimm scaling. In particular (i) for shell relaxation a pronounced peak in the reduced relaxation rates is observed, (ii) at the same Q value the reduced core relaxation rates exhibit a well-defined minimum, (iii) under average contrast conditions the low Q increase in the reduced rates sets in already at intermediate Q values, and (iv) compared to the star core the high Q increase of the reduced rates for the fully labeled star is displaced toward lower Q values. While also the long-time decay for star shell and fully labeled star is satisfactorily described by the dynamic structure factor of a Zimm chain, the core relaxation is strongly retarded at longer times.

The obtained relaxation rates were compared with the Gaussian and the structural model of section 2: (1) Qualitatively, the Q dependencies of the reduced relaxation rates can already be accounted for by the Gaussian approach. (2) Quantitatively, nearly perfect agreement is reached on the basis of the structural model that evaluates the dynamic response in terms of the measured partial structure factors. In particular in the intermediate-Q range where the static cross sections exhibit the most pronounced structure, the improvement of the data description is most significant. (3) While the Q dependence of the observed relaxation rates is remarkably well accounted for by the star architecture, the time scale of relaxation is slowed down progressively from the shell to the core, indicating the presence of hydrodynamic screening.

In conclusion, for the example of star molecules, this work has demonstrated the direct relation between the architecture of polymeric systems and their initial dynamic response. This relationship may be evaluated in detail in terms of the RPA approach. Thus, at short times the dynamics mirror the structural peculiarities of the system, though the time scale of relaxation is influenced also by essentially dynamic features like hydrodynamic screening. At longer times it appears that further dynamic effects such as interarm entanglements come into play that cannot be predicted on the basis of the structure alone.

Acknowledgment. B.E. acknowledges financial support by the Bundesminister für Forschung und Technologie (BMFT) of the Federal Republic of Germany. We benifitted from discussions with G. Grest.

References and Notes

(1) de Gennes, P.-G. *Scaling Concepts in Polymer Physics*; Cornell University Press: Ithaca, NY, 1979.
(2) des Cloiseaux, J.; Jannick, G. *Les Polymères en Solution*, Les Editions de Physique: Paris, 1987.
(3) Daoud, M.; Cotton, J. P. *J. Phys. (Français)* **1982**, *43*, 531.
(4) Birshtein, T. M.; Zhulina, E. B. *Polymer* **1984**, *25*, 1453.
(5) Birshtein, T. M.; Zhulina, E. B.; Borisov, O. V. *Polymer* **1986**, *27*, 1078.
(6) Burchard, W. *Adv. Polym. Sci.* **1983**, *48*, 1.
(7) Grest, G.; Kremer, K.; Witten, T. A. *Macromolecules* **1987**, *20*, 1376.
(8) Burchard, W.; Kajiwara, K.; Nerger, D.; Stockmayer, W. H. *Macromolecules* **1984**, *17*, 222.
(9) Benoit, H.; Hadziioannou, G. *Macromolecules* **1988**, *21*, 1449.
(10) Benoit, H.; Wu, W.; Benmouna, M. D.; Mozer, B.; Bauer, B.; Lapp, A. *Macromolecules* **1985**, *18*, 986.
(11) Akcasu, A. Z.; Benmouna, M.; Benoit, H. *Polymer* **1986**, *27*, 1935.
(12) See, e.g.: Chen, X.; Xu, Z.; von Merwall, E.; Sueng, N.; Hadjichristidis, N.; Fetters, L. J. *Macromolecules* **1984**, *17*, 1343.
(13) Huber, K.; Burchard, W.; Fetters, L. J. *Macromolecules* **1984**, *17*, 541.
(14) Richter, D.; Stühn, B.; Ewen, B.; Nerger, D. *Phys. Rev. Lett.* **1987**, *58*, 2462.
(15) Khorramion, B. A.; Stivala, S. S. *Polym. Commun.* **1986**, *27*, 184.
(16) Richter, D.; Farago, B.; Fetters, L. J.; Huang, J. S.; Ewen, B. Proceedings of the Workshop on Molecular Basis of Polymer Networks. *Springer Proceedings in Physics*, in press.

(17) Richter, D.; Farago, B.; Huang, J. S.; Fetters, L. J.; Ewen, B. *Macromolecules* **1989**, *22*, 468.
(18) de Gennes, P.-G. *Physica (Utrecht)* **1959**, *25*, 825.
(19) Kajiwara, K.; Burchard, W. *Polymer* **1981**, *22*, 1621.
(20) Akcasu, A. Z.; Benmouna, M.; Hammouda, B. *J. Chem. Phys.* **1984**, *80*, 2762.
(21) Benmouna, M.; Duval, M.; Borsali, R. *J. Polym. Sci., Polym. Phys. Ed.* **1987**, *25*, 1839.
(22) Farnoux, B. *Ann. Phys.* **1976**, *1*, 73.
(23) Kirkwood, J. G. *J. Polym. Sci.* **1954**, *12*, 1.
(24) Akcasu, Z. A.; Gurol, H. *J. Polym. Sci., Polym. Phys. Ed.* **1976**, *14*, 1.
(25) Burchard, W.; Schmidt, M.; Stockmayer, W. H. *Macromolecules* **1980**, *13*, 580.
(26) Bauer, B. J.; Fetters, L. J.; Graessley, W. W.; Hadjichristidis, N.; Quack, G. *Macromolecules* **1989**, *22*, 2337.
(27) Hadjichristidis, N.; Guyot, A.; Fetters, L. J. *Macromolecules* **1978**, *11*, 668.
(28) Hadjichristidis, N.; Fetters, L. J. *Macromolecules* **1980**, *13*, 191.
(29) Morton, M.; Fetters, L. J. *Rubber Chem. Technol.* **1975**, *48*, 359.
(30) The assertion has appeared that commercial *tert*-butyllithium is "much more unstable than other butyllithium isomers and readily decomposes". van Beylen, M.; Bywater, S. W.; Smets, G.; Szwarc, M.; Worsfold, D. J. *Adv. Polym. Sci.* **1988**, *86*, 87. If true, the use of this organolithium would be unsuitable for the preparation of model star polymers as a consequence of the resulting lack of control over arm molecular weight and the potential capacity of the decomposition products to react with the chlorosilane linking sites. Suffice it to note that in our hands commercial *tert*-butyllithium has exhibited excellent stability at room temperature. This observation is in accord with the report that pentane solutions showed "no loss in assay (by the oxidimetric technique) after one month at room temperature": Bach, R. O.; Kamienski, C. W.; Ellestad, R. B. *Encyclopedia of Chemical Technology*; 2nd ed.; John wiley & Sons: New York, 1967; Vol. 12, p 529. Under identical conditions *s*-butyllithium decomposes at ca 1.2% per week.
(31) Huber, K.; Burchhard, W.; Bantle, S.; Fetters, L. J. *Polymer* **1987**, *28*, 1997.
(32) Mezei, F. In *Lecture Notes in Physics*; Mezei, F., Ed.; Springer Verlag: Berlin, Heidelberg, New York, 1980; Vol. 128.
(33) Dubois-Violette, E.; de Gennes, P.-G. *Physics (Long Island, NY)* **1967**, *3*, 181.
(34) At asymptotically high Q for any chain statistics the Zimm model always reveals $\Omega \sim Q^3$. Only the proportionality factor depends on the fractal dimension of the polymer. In order to be able to compare with other results on dilute polymer solutions we have assumed swollen chain statistics at high Q.
(35) Richter, D.; Binder, K.; Ewen, B.; Stuhn, B. *J. Phy. Chem.* **1984**, *88*, 6618. The comparison of the nonpreaveraged theoretical result of a swollen chain with the experimentally observed characteristic frequencies yields a factor of 1.56.
(36) Grest, G. S.; Kremer, K.; Milner, S. T.; Witten, T. A. *Macromolecules* **1989**, *22*, 1904.

Photoinitiated Block Copolymer Formation Using Dithiocarbamate Free Radical Chemistry

S. Richard Turner* and Richard W. Blevins

Corporate Research Laboratories, Eastman Kodak Company, Rochester, New York 14650-2110. *Received April 28, 1989; Revised Manuscript Received September 18, 1989*

ABSTRACT: Photoinitiated block copolymer formation from macromolecules terminated with dithiocarbamate end groups was studied. In most experiments results consistent with those reported by Otsu et al. were observed. A previously unreported side reaction, leading to decomposition of the dithiocarbamate end groups, was observed. The extent of this reaction appeared to depend on the stability of the incipient macroradical formed during photolysis. Statistical mixtures of homopolymers and block copolymers were formed during the addition of methyl methacrylate to poly(styrene) and styrene to poly(methyl methacrylate). The dithiocarbamate radical did not readily initiate the polymerization of ethyl acrylate or butyl acrylate, thus relatively clean block copolymers formed when these monomers were added to polystyrene.

Introduction

Most addition polymers with complex architectures, i.e., blocks, stars, etc., are prepared by living anionic, cationic, or group-transfer polymerization techniques. The control of architecture by free radical techniques has been a synthetic goal for many years because there are a large variety of monomers that polymerize by free radicals that do not do so via ionic techniques. In general, the high reactivity and nonselectivity of free radicals make it difficult to achieve block copolymers with the same level of control and purity as can be obtained by using the anionic, cationic, and group-transfer processes. "Living" free radical chemistry based on the photolysis of "iniferter" dithiocarbamate compounds has been described as an attractive technique for preparing simple block copolymers and more complex polymer architectures.[1] This report describes our results with this technique.

Experimental Section

Tetraethylthiuram disulfide was obtained from Aldrich and recrystallized from methanol prior to use. Xylenyl dithiocarbamate (XDC) and benzyl dithiocarbamate were prepared as described by Otsu in ref 6. Monomers were purified by removing inhibitor with an appropriate column obtained from Scientific Polymer Products followed by fractional distillation. Magnetically stirred crimp-top borosilicate glass bottles were used as polymerization vessels. The contents were sparged with argon and then sealed. Photolysis reactions were conducted with a 250-W sunlamp behind a 3-cm-thick infrared filter of glass plates with a constant flow of water between them. The temperature of the polymerization samples behind this barrier was maintained at 20–25 °C. Preparation of dithiocarbamate-containing end-capped homopolymers was done thermally at 60 °C in bottles under argon with tetraethyldithiuram disulfide as the

0024-9297/90/2223-1856$02.50/0